PERGAMON

International Journal of Heat and Mass Transfer 43 (2000) 705–724

International Journal of HEAT and MASS TRANSFER

www.elsevier.com/locate/ijhmt

Subcritical transitions to chaos and hysteresis in a fluid layer heated from below

Peter Vadasz*

Department of Mechanical Engineering, University of Durban-Westville, Private Bag X54001, Durban 4000, South Africa

Received 14 May 1998; received in revised form 18 May 1999

Abstract

The route to chaos in a fluid layer heated from below is investigated by using the weak non-linear theory as well as Adomian's decomposition method to solve a system of ordinary differential equations which result from a truncated Galerkin representation of the governing equations. This representation yields the familiar Lorenz equations. While the weak non-linear method of solution provides significant insight to the problem, to its solution and corresponding bifurcations and other transitions, it is limited because of its local domain of validity, which in the present case is in the neighbourhood of any one (but only one) of the two steady state convective solutions. This method is expected to loose accuracy and gradually breakdown as one moves away from this neighbourhood. On the other hand, Adomian's decomposition method provides an analytical solution to the problem in terms of an infinite power series. The practical need to evaluate numerical values from the infinite power series, the consequent series truncation, and the practical procedure to accomplish this task transform the otherwise analytical results into a computational solution achieved up to a finite accuracy. The transition from the steady solution to chaos is analysed by using both methods and their results are compared, showing a very good agreement in the neighbourhood of the convective steady solutions. The analysis explains the computational results, which indicate a transition from steady convection to chaos via a solitary limit cycle followed by a homoclinic explosion at a subcritical value of a Rayleigh number. A transient analysis of the amplitude equation obtained from the weak non-linear solution reveals the mechanism by which the Hopf bifurcation becomes subcritical. A simple explanation of the well-known experimental phenomenon of hysteresis in the transition from steady convection to chaos and backwards from chaos to steady state is provided in terms of the present analysis results.

Keywords: Chaos; Free convection; Weak turbulence; Lorenz equations

1. Introduction

The investigation of free convection in a fluid layer heated from below is receiving extensive attention due to its wide field of applications in different disciplines such as atmospheric sciences, oceanography and engineering.

There are different approaches to analyse the non-linear convection problem leading to different degrees of insight into the variety of phenomena and the corresponding dynamics of the system as the Rayleigh number increases. One such approach was adopted by Lorenz [1] (see also [2,3]). While the truncated Lorenz equations are limited either to moderate Rayleigh

* Tel.: +27-31-204-4873; fax: +27-31-204-4002.
E-mail address: vadasz@pixie.udw.ac.za (P. Vadasz).

0017-9310/00/$ - see front matter
PII: S0017-9310(99)00173-8

Nomenclature

$\hat{\boldsymbol{e}}_x$ unit vector in the x-direction
$\hat{\boldsymbol{e}}_y$ unit vector in the y-direction
$\hat{\boldsymbol{e}}_z$ unit vector in the z-direction
$\hat{\boldsymbol{e}}_g$ unit vector in the direction of gravity
$\hat{\boldsymbol{e}}_n$ unit vector normal to the boundary, positive outwards
g_* gravity acceleration
H_* the height of the layer
p reduced pressure (dimensionless)
Pr Prandtl number, equals ν_*/α_*
$\boldsymbol{V}$ dimensionless velocity vector equals $u\hat{\boldsymbol{e}}_x + v\hat{\boldsymbol{e}}_y + w\hat{\boldsymbol{e}}_z$
r absolute value of the complex amplitude
r_0 initial condition of r
R scaled Rayleigh number, equals Ra/Ra_c
R_t transitional value of R, corresponding to the transition from steady convection to chaos, defined by Eq. (42)
R_0 critical value of R for the loss of linear stability of the steady convection solution
Ra Rayleigh number, equals $\beta_*\Delta T_c g_* H_*^3/\alpha_*\nu_*$
Ra_c critical value of Rayleigh number for the loss of linear stability of the motionless solution
Ra_0 critical value of Rayleigh number for the loss of linear stability of the steady convection solution
$\hat{t}$ time
T dimensionless temperature, equals $(T_*-T_C)/(T_H-T_C)$
T_C coldest wall temperature
T_H hottest wall temperature
u horizontal x component of the velocity
v horizontal y component of the velocity
w vertical component of the velocity
x horizontal length co-ordinate
X rescaled amplitude $\tilde{A}_{11}$, Eq. (10)
y horizontal width co-ordinate
Y rescaled amplitude $\tilde{B}_{11}$, Eq. (10)
z vertical co-ordinate
Z rescaled amplitude $\tilde{B}_{02}$, Eq. (10).

Greek symbols
α_* thermal diffusivity
β relaxation time parameter in Eq. (34)
β_T dimensionless form of the thermal expansion coefficient
β_* thermal expansion coefficient
ΔT_c characteristic temperature difference
ε asymptotic expansion parameter, defined in the text following Eq. (16)
$\dot{\theta}$ higher-order frequency correction
ν_* fluid's kinematic viscosity
ξ a parameter in Eq. (36), equals ε^2/φ
ρ density, dimensionless
ρ_0 reference value of density, dimensional
τ long time scale
φ coefficient of the non-linear term in the amplitude equation (34)
χ a parameter in Eq. (36), equals φ/β
ψ stream function.

Subscripts
c characteristic values
cr critical values
C related to the coldest wall
H related to the hottest wall
t transitional values
* dimensional values.

Superscripts
* complex conjugate.

numbers or to represent the solution in the interior, excluding boundary layers which develop at high values of Ra, Malkus [4] showed that this set of three equations decouple from the rest (with exact closure), at least in the sense of weighted residuals.

In the present paper the same model is adopted to present the solution analytically by using Adomian's decomposition method [5,6]. The resulting solutions are an infinite power series which needs to be truncated in order to evaluate their numerical values. This truncation linked to a practical procedure for evaluating these solutions at specific values of time leads to steady, periodic and chaotic flow regimes. In particular it is noticed that the transition to chaos when the initial conditions are not too far away from any one of the convective steady state solutions passes through a limit cycle at a particular subcritical value of the Rayleigh number. Here the term 'subcritical' is used in the context of the transition from steady convection to a non-periodic state, typically referred to as chaotic, and the critical value of the Rayleigh number is the value at which this transition to chaos is predicted by the linear stability analysis of the convective steady state solutions. Similar results were presented by Vadasz and Olek [7] for the corresponding problem of gravity driven convection in porous media and by Vadasz and Olek [8] for centrifugally induced convection in a rotating porous layer. In particular the com-

putational recovery of a periodic solution (limit cycle) at a particular subcritical value of the Rayleigh number followed immediately by chaos, is in apparent contrast to available weak non-linear analysis results [9,10] of the Lorenz equations which suggest that such a limit cycle solution is unstable. Wang et al. [9] and Yuen and Bau [10], while presenting methods of controlling chaos and rendering a subcritical Hopf bifurcation supercritical, respectively, in a thermal convection loop, also present a summary of the sequence of transitions in the Lorenz system leading to chaos. In particular they identify a well-known experimental and numerical phenomenon of hysteresis which can be described as follows: when increasing the Rayleigh number gradually by approaching the critical value from below the transition to chaos occurs at $Ra = Ra_0$, while repeating the same procedure but approaching Ra_0 from above the transition from chaos to the stationary solution occurs at a value of $Ra < Ra_0$. Sparrow [2] shows that for the Lorenz system analysed around the origin (i.e. around the solution corresponding to the motionless state) the transition to chaos is via a homoclinic explosion. He then makes the reasonable deduction that the homoclinic orbit, which exists just at the point where the solution orbiting around one steady solution turns towards the other steady solution, belongs to the subcritical Hopf bifurcation which was obtained at $Ra = Ra_0$ (the two steady solutions correspond to the two branches of the pitchfork bifurcation obtained at the first transition from a motionless state to convection and consist of convection cells rotating clockwise or counter-clockwise).

The objective of the present paper is to extend the above mentioned analyses and report additional results of non-linear solutions to this problem obtained via the weak non-linear analysis around the steady convective states and via the Adomian's decomposition method [5,6]. Similar solutions are presented by Vadasz [11] for convection in a porous layer heated from below. In particular these results provide an explanation for the computational recovery of the unstable limit cycle solution at a subcritical value of the Rayleigh number on the threshold of the transition to chaos and a simple explanation of the hysteresis phenomenon linked to the transition from steady convection to chaos and backwards to steady convection.

This is accomplished first by undertaking a weak non-linear analysis leading to a complex amplitude equation which is being analysed to identify further details related to the subcritical Hopf bifurcation. Thereafter, the solution to the problem is obtained by adopting Adomian's decomposition method [5,6] to solve the set of ordinary differential equations. Although the solution to the problem using this method is analytical, the evaluation of the resulting infinite series, including the series truncation is a computational procedure. We will, therefore, refer to the results obtained via the weak non-linear analysis as analytical (though local) and to the results obtained via the Adomian's decomposition method as computation (as distinct from numerical) to stress the fact that the latter are also obtained from an analytical solution which needed to be computed up to a finite accuracy.

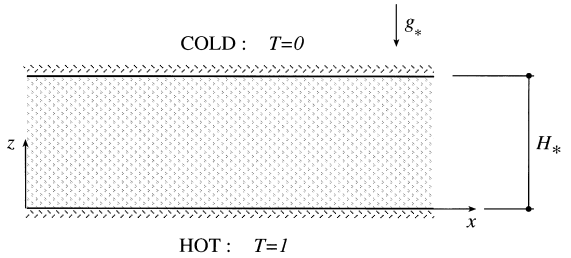

Fig. 1. A fluid layer subject to gravity and heated from below.

Adomian's decomposition method was shown to provide extremely accurate results for a wide range of non-linear problems (see [12,13]), some of which have closed form analytical solutions and the comparison between the decomposition method and the known analytical (or alternatively numerical) results as presented by Olek [12,13] agreed up to 14 significant digits.

2. Problem formulation

A very long and narrow fluid layer subject to gravity and heated from below, as presented in Fig. 1, is considered. A Cartesian co-ordinate system is used such that the vertical axis z is collinear with gravity, i.e. $\hat{\boldsymbol{e}}_g = -\hat{\boldsymbol{e}}_z$. A linear relationship between density and temperature is assumed and can be presented in the following dimensionless form $\rho = 1 - \beta_T T$, where $\beta_T = \beta_*(T_H - T_C)$ and β_* represents the dimensional thermal expansion coefficient while $(T_H - T_C)$ is the temperature difference between the hot and cold walls of the fluid layer. The Boussinesq approximation is applied indicating that density variations are neglected everywhere except for the gravity term in the momentum equation. Subject to these conditions the following dimensionless set of governing equations is obtained

$$\nabla \cdot \boldsymbol{V} = 0 \tag{1}$$

$$\frac{1}{Pr}\left[\frac{\partial}{\partial \hat{t}} + \boldsymbol{V} \cdot \nabla\right]\boldsymbol{V} = -\nabla p + \nabla^2 \boldsymbol{V} + Ra\ T\hat{\boldsymbol{e}}_z \tag{2}$$

$$\frac{\partial T}{\partial \hat{t}} + \boldsymbol{V}\cdot\nabla T = \nabla^2 T \tag{3}$$

Eqs. (1)–(3) are presented in a dimensionless form. The values α_*/H_*, $\rho_0\alpha_*^2/H_*^2$, and $\Delta T_c=(T_H-T_C)$ are used to scale the velocity components (u_*, v_*, w_*), reduced pressure (p_*), and temperature variations (T_*-T_C), respectively, where α_* is the thermal diffusivity and ρ_0 is a reference value of density. The height of the layer H_* was used for scaling the variables x_*, y_*, z_* and H_*^2/α_* for scaling the time t_*. Accordingly, $x=x_*/H_*$, $y=y_*/H_*$ and $z=z_*/H_*$ and $\hat{t}=t_*\alpha_*/H_*^2$. In Eq. (2) $Pr=\nu_*/\alpha_*$ is the Prandtl number and Ra is the Rayleigh number defined in the form $Ra=\beta_*\Delta T_c g_* H_*^3/\alpha_*\nu_*$.

We consider the horizontal boundaries to be stress free (i.e. no tangential shear stress), hence, the solution must follow the impermeability conditions $\boldsymbol{V}\cdot\hat{\boldsymbol{e}}_n=0$ and the stress free conditions $\partial u/\partial z=\partial v/\partial z=\partial^2 w/\partial z^2=0$ on these boundaries, where $\hat{\boldsymbol{e}}_n$ is a unit vector normal to the boundary. The temperature boundary conditions are: $T=1$ at $z=0$, $T=0$ at $z=1$.

For convective rolls having axes parallel to the shorter dimension (i.e. y) $v=0$, and the governing equations can be presented in terms of a stream function defined by $u=-\partial\psi/\partial z$ and $w=\partial\psi/\partial x$, which upon applying the curl($\nabla\times$) operator on Eq. (2) yields the following system of partial differential equations from Eqs. (1)–(3)

$$\left[\frac{1}{Pr}\left(\frac{\partial}{\partial\hat{t}}+\frac{\partial\psi}{\partial z}\frac{\partial}{\partial x}-\frac{\partial\psi}{\partial x}\frac{\partial}{\partial z}\right)-\nabla^2\right]\nabla^2\psi = Ra\frac{\partial T}{\partial x} \tag{4}$$

$$\frac{\partial T}{\partial\hat{t}}-\frac{\partial\psi}{\partial z}\frac{\partial T}{\partial x}+\frac{\partial\psi}{\partial x}\frac{\partial T}{\partial z}=\frac{\partial^2 T}{\partial x^2}+\frac{\partial^2 T}{\partial z^2} \tag{5}$$

where the two-dimensional Laplacian operator is defined in the form $\nabla^2\equiv\partial^2/\partial x^2+\partial^2/\partial z^2$ and the boundary conditions for the stream function are $\psi=\partial\psi/\partial z=0$ on the horizontal boundaries.

The set of partial differential equations (4) and (5) form a non-linear coupled system which together with the corresponding boundary conditions accepts a basic motionless conduction solution. To obtain the complete solution to the non-linear coupled system of partial differential equations (4) and (5) we represent the stream function and temperature in the form

$$\psi = A_{11}(\hat{t})\sin(\kappa x)\sin(\pi z) \tag{6}$$

$$T = 1 - z + B_{11}(\hat{t})\cos(\kappa x)\sin(\pi z) + B_{02}(\hat{t})\sin(2\pi z) \tag{7}$$

This representation is equivalent to a Galerkin expansion of the solution in both x and z directions, truncated when $i+j=2$, where i is the Galerkin summation index in the x-direction and j is the Galerkin summation index in the z-direction. Substituting (6) and (7) into the Eqs. (4) and (5), multiplying the equations by the orthogonal eigenfunctions corresponding to (6) and (7) and integrating them over the height of the domain and over the wavelength of the convection cell in the vertical and horizontal directions, respectively, i.e. $\int_0^{\pi/\kappa}\mathrm{d}x\int_0^1\mathrm{d}z(\ )$, yields a set of three ordinary differential equations for the time evolution of the amplitudes in the form

$$\frac{\mathrm{d}\tilde{A}_{11}}{\mathrm{d}t} = Pr(\tilde{B}_{11}-\tilde{A}_{11}) \tag{8a}$$

$$\frac{\mathrm{d}\tilde{B}_{11}}{\mathrm{d}t} = -\tilde{B}_{11}+R\tilde{A}_{11}-\tilde{A}_{11}\tilde{B}_{02} \tag{8b}$$

$$\frac{\mathrm{d}\tilde{B}_{02}}{\mathrm{d}t} = -\lambda\tilde{B}_{02}+\tilde{A}_{11}\tilde{B}_{11} \tag{8c}$$

where the time, the amplitudes and the Rayleigh number were rescaled and the following notation was introduced

$$\tilde{A}_{11}=\frac{(\kappa/\kappa_{rc})}{[(\kappa/\kappa_{cr})^2+2]}A_{11};\quad \tilde{B}_{11}=\kappa_{cr}RB_{11};\quad \tilde{B}_{02}=\pi RB_{02};\quad R=\frac{Ra}{Ra_c} \tag{9a}$$

$$t=(\kappa^2+\pi^2)\hat{t};\quad \lambda=\frac{8}{[(\kappa/\kappa_{cr})^2+2]};\quad Ra_c=\frac{(\kappa^2+\pi^2)^3}{\kappa^2};\quad \kappa_{cr}=\frac{\pi}{\sqrt{2}} \tag{9b}$$

Eqs. 8(a–c) are the famous Lorenz equations [1,2], which yield the following convective stationary solutions $\tilde{A}_{11}=\tilde{B}_{11}=\pm[\lambda(R-1)]^{1/2}$, $\tilde{B}_{02}=(R-1)$. Rescaling the equations again with respect to their convective fixed points in the form

$$X=\frac{\tilde{A}_{11}}{\sqrt{\lambda(R-1)}}\quad Y=\frac{\tilde{B}_{11}}{\sqrt{\lambda(R-1)}}\quad Z=\frac{\tilde{B}_{02}}{(R-1)} \tag{10}$$

provides the following set of scaled equations

$$\dot{X} = Pr(Y-X) \tag{11}$$

$$\dot{Y} = RX - Y - (R-1)XZ \tag{12}$$

$$\dot{Z} = \lambda(XY-Z) \tag{13}$$

where the dots ($\dot{}$) denote time derivatives $\mathrm{d}(\ )/\mathrm{d}t$. By using the wavenumber corresponding to the convection

threshold, i.e. κ_{cr}, in the definitions of λ and Ra_c [Eq. (9)] yields $\lambda = 8/3$ and $Ra_c = 27\pi^4/4$.

3. Weak non-linear analysis — local solution

Before we proceed to present the global solution to the problem, a weak non-linear analysis of the system (11)–(13) is undertaken, which emphasises analytically some local aspects of the solution around the convection fixed points and provides insight and simple explanations to the computational results presented in the following section.

3.1. The asymptotic expansion and amplitude equation

The stationary (fixed) points of the system (11)–(13) are the convective solutions $X_S = Y_S = \pm 1$, $Z_S = 1$ and the motionless solution $X_S = Y_S = Z_S = 0$ (occasionally referred to as the origin). The expansion around the motionless stationary solution yields the familiar results of a pitchfork bifurcation from a motionless state to convection at $R = 1$. We expand now the dependent variables around the convection stationary points in a form similar to Yuen and Bau [10]

$$X = X_S + \varepsilon X_1 + \varepsilon^2 X_2 + \varepsilon^3 X_3 + \cdots \tag{14}$$

$$Y = Y_S + \varepsilon Y_1 + \varepsilon^2 Y_2 + \varepsilon^3 Y_3 + \cdots \tag{15}$$

$$Z = Z_S + \varepsilon Z_1 + \varepsilon^2 Z_2 + \varepsilon^3 Z_3 + \cdots \tag{16}$$

We also expand R in a finite series of the form $R = R_0(1+\varepsilon^2)$ which now defines the small expansion parameter as $\varepsilon^2 = (R-R_0)/R_0$, where R_0 is the value of R where the stationary convective solutions loose their stability in the linear sense. Therefore, the present weak non-linear analysis is expected to be restricted to initial conditions sufficiently close to any one of the convective fixed points. Introducing a long time scale $\tau = \varepsilon^2 t$ and replacing the time derivatives in Eqs. (11)–(13) with $\mathrm{d}/\mathrm{d}t \to \mathrm{d}/\mathrm{d}t + \varepsilon^2\ \mathrm{d}/\mathrm{d}\tau$, yields a hierarchy of ordinary differential equations at the different orders. The leading order provides the stationary solutions, while at order ε we get the familiar homogeneous linearised system

$$\dot{X}_1 - Pr(Y_1 - X_1) = 0 \tag{17}$$

$$\dot{Y}_1 - [X_1 - Y_1 \mp (R_0 - 1)Z_1] = 0 \tag{18}$$

$$\dot{Z}_1 - \lambda(\pm X_1 \pm Y_1 - Z_1) = 0 \tag{19}$$

where the $\pm$ upper or under-sign corresponds to the selected stationary convective point, either $X_S = Y_S = 1$, $Z_S = 1$ corresponding to the upper-sign, or $X_S = Y_S = -1$, $Z_S = 1$ corresponding to the under-sign. The following stages will focus on the solution around $X_S = Y_S = 1$, $Z_S = 1$, hence, the upper-sign holds. Similar equations hold for the other stationary point. The solutions to the linear set (17)–(19) have the form:

$$\begin{aligned} X_1 &= a_1\, \mathrm{e}^{i\sigma_0 t} + a_1^*\, \mathrm{e}^{-i\sigma_0 t};\\ Y_1 &= b_1\, \mathrm{e}^{i\sigma_0 t} + b_1^*\, \mathrm{e}^{-i\sigma_0 t};\\ Z_1 &= c_1\, \mathrm{e}^{i\sigma_0 t} + c_1^*\, \mathrm{e}^{-i\sigma_0 t} \end{aligned} \tag{20}$$

where the coefficients $a_1(\tau)$, $a_1^*(\tau)$, $b_1(\tau)$, $b_1^*(\tau)$, $c_1(\tau)$ and $c_1^*(\tau)$ are allowed to vary over the long time scale τ and $\pm i\sigma_0$ are the imaginary parts of the complex eigenvalues corresponding to the linear system at marginal stability (i.e. the real part of the eigenvalues is 0). They are related to Pr by the equation $\sigma_0^2 = 2\lambda\ Pr(Pr + 1)/(Pr-\lambda-1)$, which can be established by working out the relationships between the $O(\varepsilon)$ coefficients in the solution (20). These relationships are obtained by substituting the solutions (20) into the linear equations (17)–(19) and yield

$$b_1 = \frac{(Pr + i\sigma_0)}{Pr} a_1; \quad b_1^* = \frac{(Pr - i\sigma_0)}{Pr} a_1^* \tag{21}$$

$$\begin{aligned} c_1 &= \frac{\sigma_0[\sigma_0 - i(Pr+1)]}{Pr(R_0 - 1)} a_1;\\ c_1^* &= \frac{\sigma_0[\sigma_0 + i(Pr+1)]}{Pr(R_0 - 1)} a_1^* \end{aligned} \tag{22}$$

The equation for R_0 is also obtained in the form $R_0 = Pr(Pr+\lambda+3)/(Pr-\lambda-1)$. For $\lambda = 8/3$ and $Pr = 10$ the corresponding value of R_0 is $R_0 \cong 24.737$.

At order $O(\varepsilon^2)$ the equations have the form

$$\dot{X}_2 - Pr(Y_2 - X_2) = 0 \tag{23}$$

$$\dot{Y}_2 - [X_2 - Y_2 - (R_0 - 1)Z_2] = -(R_0 - 1)X_1 Z_1 \tag{24}$$

$$\dot{Z}_2 - \lambda(X_2 + Y_2 - Z_2) = \lambda X_1 Y_1 \tag{25}$$

The system (23)–(25) is a non-homogeneous version of the system (17)–(19), sharing the same homogeneous operator. Therefore, the homogenous solutions to (23)–(25) have the same form as Eq. (20) (with different coefficients) to which the forcing functions on the right-hand-side of (23)–(250 contribute particular solutions. The complete solution at this order has the form

$$X_2 = a_2\,\mathrm{e}^{i\sigma_0 t} + a_2^*\,\mathrm{e}^{-i\sigma_0 t} + a_{22}\,\mathrm{e}^{i2\sigma_0 t} + a_{22}^*\,\mathrm{e}^{-i2\sigma_0 t} + a_{20} \tag{26a}$$

$$Y_2 = b_2\,\mathrm{e}^{i\sigma_0 t} + b_2^*\,\mathrm{e}^{-i\sigma_0 t} + b_{22}\,\mathrm{e}^{i2\sigma_0 t} + b_{22}^*\,\mathrm{e}^{-i2\sigma_0 t} + b_{20} \tag{26b}$$

$$Z_2 = c_2\,\mathrm{e}^{i\sigma_0 t} + c_2^*\,\mathrm{e}^{-i\sigma_0 t} + c_{22}\,\mathrm{e}^{i2\sigma_0 t} + c_{22}^*\,\mathrm{e}^{-i2\sigma_0 t} + c_{20} \tag{26c}$$

where the first two terms in each one of these equations represent the homogeneous solution while the remaining three correspond to the particular solution forced by the right-hand-side terms in Eqs. (23)–(25). The relationships between b_2, c_2 and a_2, and between b_2^*, c_2^* and a_2^* are identical to Eqs. (21) and (22) while the relationships between the coefficients of the particular solutions and the $O(\varepsilon)$ coefficients are obtained upon substitution of the particular solutions into Eqs. (23)–(25) and yield

$$a_{20} = b_{20} = -\frac{[\sigma_0^2 + Pr(R_0 - 1)]}{Pr(R_0 - 1)} a_1 a_1^*; \qquad c_{20} = -\frac{2\sigma_0^2}{Pr(R_0 - 1)} a_1 a_1^* \tag{27}$$

$$a_{22} = -p^0 a_1^2; \quad b_{22} = -q^0 a_1^2; \quad c_{22} = -s^0 a_1^2 \tag{28}$$

where p^0, q^0 and s^0 are given by the following equations

$$p^0 = \frac{[\sigma_0^2(2\ Pr + \lambda + 2) + Pr(R_0 - 1)] + i\sigma_0[2\sigma_0^2 + \lambda(R_0 - Pr - 2)]}{2\{[\lambda\ Pr(R_0 - 1) - 2\sigma_0^2(Pr + \lambda + 1)] + i\sigma_0[\lambda(R_0 + Pr) - 4\sigma_0^2]\}} \tag{29a}$$

$$q^0 = \frac{(Pr + i2\sigma_0)}{Pr} p^0 \tag{29b}$$

$$s^0 = \frac{\lambda\sigma_0(Pr + i\sigma_0)[3\sigma_0 - i2(Pr + 1)]}{Pr\{[\lambda\ Pr(R_0 - 1) - 2\sigma_0^2(Pr + \lambda + 1)] + i\sigma_0[\lambda(R_0 + Pr) - 4\sigma_0^2]\}} \tag{29c}$$

with equivalent relationships for their complex conjugate coefficients a_{22}^*, b_{22}^* and c_{22}^*.

The equations at order $O(\varepsilon^3)$ have the form

$$\dot{X}_3 - Pr(Y_3 - X_3) = -\frac{\mathrm{d}X_1}{\mathrm{d}\tau} \tag{30}$$

$$\dot{Y}_3 - [X_3 - Y_3 - (R_0 - 1)Z_3] = -\frac{\mathrm{d}Y_1}{\mathrm{d}\tau} - R_0 Z_1 - (R_0 - 1)(X_1 Z_2 + X_2 Z_1) \tag{31}$$

$$\dot{Z}_3 - \lambda(X_3 + Y_3 - Z_3) = -\frac{\mathrm{d}Z_1}{\mathrm{d}\tau} + \lambda(X_1 Y_2 + X_2 Y_1) \tag{32}$$

Eqs. (30)–(32) have the same homogeneous operator as the $O(\varepsilon)$ solutions, while the right-hand-side forcing functions, which depend on the solutions evaluated at lower orders, produce particular solutions at this order, provided a solvability condition is fulfilled. The solvability condition is obtained in order to prevent terms of the form $\mathrm{e}^{i\sigma_0 t}$ and $\mathrm{e}^{-i\sigma_0 t}$ on the right-hand-side of Eqs. (30)–(32) to resonate the homogeneous operator, hence, forcing secular solutions of the form $t\,\mathrm{e}^{i\sigma_0 t}$ and $t\,\mathrm{e}^{-i\sigma_0 t}$ which are not bounded as $t \to \infty$. Hence, the coefficients of these secular terms on the right-hand-side of (30)–(32) must vanish, a requirement which provides a constraint on the amplitudes at $O(\varepsilon)$ in the form of an amplitude equation.

3.2. The Hopf bifurcation and limit cycle solution

The solvability condition is obtained by first decoupling the system (30)–(32) and then requiring the coefficient of the resonating terms to vanish, a procedure which yields the amplitude equation in the form

$$\frac{\mathrm{d}a}{\mathrm{d}t} = h_{21}[\varepsilon^2 - h_{32} a a^*]a \tag{33}$$

and a similar equation for a^*, where in Eq. (33) $a = \varepsilon a_1$, $a^* = \varepsilon a_1^*$ and h_{21}, h_{32} are complex coefficients which depend on Pr, σ_0, R_0, p^0, q^0 and s^0. Their lengthy expressions are skipped here. The coefficient of the non-linear term in Eq. (33) plays a role of a particular importance as it controls the direction of the Hopf bifurcation which results from the post-transient solution to Eq. (33). To observe this point further it is convenient to represent Eq. (33) for the complex amplitude, a, as a set of two equations for the absolute value of the amplitude, $r = |a|$, and its phase, θ, in the

form: $a=r\ \mathrm{e}^{i\theta}$, $a^*=r\ \mathrm{e}^{-i\theta}$, with $aa^*=r^2$. Substituting this representation in Eq. (33) yields

$$\beta\frac{\mathrm{d}r}{\mathrm{d}t}=[\varepsilon^2-\varphi r^2]r \tag{34}$$

$$\frac{\mathrm{d}\theta}{\mathrm{d}t}=m_{21}\varepsilon^2-m_{31}r^2 \tag{35}$$

where the following notation was introduced to separate between the real and imaginary parts of the coefficients in Eq. (33) $h_{21}=h^0_{21}+im_{21}$, $h_{31}=h^0_{31}+im_{31}$ and $\beta=1/h^0_{21}$, $\varphi=h^0_{31}/h^0_{21}$.

Now it can be observed that when the coefficient of the non-linear term, φ, is positive the Hopf bifurcation is forward (i.e. supercritical) while a negative value of φ yields an inverse bifurcation (i.e. subcritical). The coefficient, φ, was evaluated as a function of Pr for $\lambda=8/3$ allowing to establish that its value is negative over the whole domain of validity of the Hopf bifurcation. The relaxation time, β, was also evaluated as a function of Pr indicating that it is positive for $Pr\geq 11/3$. Except for a range of Pr values slightly larger than 2.5 and slightly smaller than 11/3, where the relaxation time is negative and the bifurcation seems to be supercritical, the values of β are always positive. Note that values of $Pr\leq 11/3$ are not consistent with the Hopf bifurcation and with the solutions considered here, as can be observed from the equation for R_0 [see text following Eq. (22)]. For such values of Pr the solution of this system decays to the stationary points. We can, therefore, confirm previously suggested results [2,9,10] related to the Lorenz equations, that the Hopf bifurcation in this system is indeed subcritical. A further analysis of the periodic solution (see the Appendix) at slightly subcritical values of R shows that this solution is unstable for $\varepsilon^2<0$ (i.e. $R<R_0$). We are, therefore, faced with a periodic solution which exists only for $\varepsilon^2<0$ (i.e. $R<R_0$) but it is not stable in this domain. However, it is at this point where the further investigation of the amplitude equation provides a marked insight into the details of this Hopf bifurcation at the point where the steady convective solutions loose their stability but the resulting periodic solution unfolding from the amplitude equation is unstable for $R<R_0$ and does not exist when $R>R_0$. The post-transient amplitude solution is obtained from Eq. (34) in the form $r^2=\varepsilon^2/\varphi$ which clearly yields a real value for the amplitude only when $\varepsilon^2\leq 0$ (i.e. $R\leq R_0$) given the already established fact that $\varphi<0$. The post-transient frequency correction, $\dot{\theta}$, can be obtained for $R\leq R_0$ by substituting the post-transient solution for r^2 into (35) in the form $\dot{\theta}=(m_{21}-m_{31}/\varphi)\varepsilon^2$. The complete solution for X, as an example, has, therefore, the form $X=1+\varepsilon r_1[\exp(i(\dot{\theta}+\sigma_0)t)+\exp(-i(\dot{\theta}+\sigma_0)t)]+O(\varepsilon^2)$ (where $r=\varepsilon r_1$). Clearly, $r=\varepsilon r_1$ needs to be much smaller than one for the asymptotic solution to be accurate. In particular the initial conditions for r, i.e. r_0, needs to be much smaller than one, providing the condition for accuracy of the weak non-linear solution in the form $r_0\ll 1$. Therefore, as the value of r_0 ceases to satisfy this condition its departure causes the accuracy of the weak non-linear solution to be lost.

3.3. Investigation of the transient solution to the amplitude equation

To gain more insight into the nature of the limit cycle and the subcriticality of the Hopf bifurcation resulting from the amplitude equation, we undertake further investigation of this equation. The major point being the question of where exactly the supercritical solution disappeared, what is the reason for its disappearance and what more can we learn about the unstable subcritical limit cycle. This is done by working out the transient solution of Eq. (34) which can be easily obtained by a simple integration. Prior to that it is convenient to introduce the following notation, which simplifies the analysis, $\chi=\varphi/\beta$ and $\xi=\varepsilon^2/\varphi$. Clearly $\chi<0$ over all the cases to be considered in this analysis, while $\xi>0$ for $\varepsilon^2<0$ (subcritical conditions), $\xi<0$ for $\varepsilon^2>0$ (supercritical conditions), and $\xi=0$ for $\varepsilon^2=0$ (critical conditions). By using this notation the amplitude Eq. (34) takes the form

$$\frac{\mathrm{d}r}{\mathrm{d}t}=\chi[\xi-r^2]r \tag{36}$$

The solution to eq. (36) is obtained by direct integration in the form $r^2=\xi\ \exp(2\xi\chi t)/[D+\exp(2\xi\chi t)]$ for $\xi\neq 0$ $(\varepsilon^2\neq 0)$ and $r^2=1/[2(\chi t-D)]$ for $\xi=0$ $(\varepsilon^2=0)$, where D is a constant of integration to be determined from the initial conditions. By introducing the initial conditions $r=r_0$ at $t=0$, the transient solutions take the form

$$r^2=\frac{\xi}{\left[1-\left(1-\frac{\xi}{r_0^2}\right)\exp(-2\xi\chi t)\right]}\quad \text{for } \xi\neq 0 \quad (\varepsilon^2\neq 0) \tag{37}$$

$$r^2=\frac{r_0^2}{[1+2r_0^2\chi t]}\quad \text{for } \xi=0\quad (\varepsilon^2=0) \tag{38}$$

Clearly, both solutions (37) and (38) are valid at $t=0$ and yield then $r^2=r_0^2$ which can be easily recovered by substituting $t=0$ in Eqs. (37) and (38). Therefore, the question which arises is what happens at a later time $t>0$ which causes these solutions to disappear when $\varepsilon^2>0$ (i.e. when $\xi<0$). To answer this question we

separate the discussion into three cases as follows: (i) the supercritical case, $\varepsilon^2 > 0$ ($\xi < 0$), (ii) the subcritical case, $\varepsilon^2 < 0$ ($\xi > 0$) and (iii) the critical case, $\varepsilon^2 = 0$ ($\xi = 0$). In all three cases it should be remembered that the value of χ is always negative, while ξ is negative, zero, or positive depending on whether the conditions are supercritical, critical or subcritical, respectively.

3.3.1. The supercritical case, $\varepsilon^2 > 0$ ($\xi < 0$)

For this case the argument of the exponent in the denominator of Eq. (37) and the value of ξ/r_0^2 are always negative. Therefore, the denominator has at $t = 0$, a negative value and this value increases until such time that the denominator vanishes causing the solution of r^2 to become infinite. To evaluate this critical time, t_{cr}, when the solution diverges we check the condition when the denominator becomes equal to zero, providing the following result

$$t_{cr} = \frac{1}{2\chi\xi} \ln\left[1 - \frac{\xi}{r_0^2}\right] \tag{39}$$

Obviously, since $\xi < 0$ in this case the argument of the natural logarithm is always greater than one, therefore, this critical time exists unconditionally in the supercritical regime, causing the amplitude solution to diverge, the significance of which will be discussed below.

3.3.2. The subcritical case, $\varepsilon^2 < 0$ ($\xi > 0$)

For this case the argument of the exponent in the denominator of Eq. (37) and the value of ξ/r_0^2 are always positive. The denominator has at $t = 0$, a positive value and this value decreases or increases depending on the value of the ratio ξ/r_0^2. To establish the conditions for the denominator of the solution (37) to become zero and cause the solution to diverge we evaluate the critical time in a similar way as for the supercritical case, providing an identical result for t_{cr} as presented in Eq. (39). However, this time, under subcritical conditions $\xi > 0$, the coefficient of the natural logarithm is negative and its argument can be greater or less than one depending on the value of ξ/r_0^2. It is easier to notice the behaviour of the solution in the subcritical case by presenting the equation for the critical time corresponding to the subcritical case in the following form, where we express explicitly the fact that $\chi < 0$

$$t_{cr} = -\frac{1}{2\,|\,\chi\,|\,\xi} \ln\left[1 - \frac{\xi}{r_0^2}\right] \tag{40}$$

From this equation it is clear that the condition for existence of a critical time is that the argument of the natural logarithm in Eq. (40) be positive and less than one, i.e. $0 < (1-\xi/r_0^2) < 1$. Otherwise, either the ln( ) function does not exist or the critical time becomes negative having no physical significance. The right-hand-side of this inequality yields: $\xi/r_0^2 > 0$, which is unconditionally satisfied under subcritical conditions ($\xi > 0$). The left-hand-side provides the following condition for existence of a critical time: $\xi/r_0^2 < 1$. The interesting fact coming out from this result is that a critical time when the limit cycle solution diverges exists in the subcritical case as well, subject to the condition $\xi/r_0^2 < 1$.

3.3.3. The critical case, $\varepsilon^2 = 0$ ($\xi = 0$)

For the critical case we use Eq. (38) and evaluate the condition for its denominator to vanish in order to establish the existence of a critical time in this case as well. One may expect it to exist on continuity arguments as its exists conditionally in the subcritical case and unconditionally in the supercritical case. From Eq. (38) it can be easily evaluated as

$$t_{cr} = -\frac{1}{2\chi r_0^2} \quad \text{for } \xi = 0 \tag{41}$$

The same result as presented in Eq. (41) can be obtained by applying the limit as $\xi \to 0$ and using the L'Hopital rule on Eq. (39) which is valid for both the subcritical and supercritical conditions. This indicates that the critical time t_{cr} as a function of ξ varies smoothly as it passes through the critical point $\xi = 0$ ($\varepsilon^2 = 0$).

The significance of the existence of a critical time when the limit cycle solution diverges is explained simply in terms of the breakdown of the asymptotic expansion which implicitly assumes (a) that the solution is local, around any one (but only one) of the fixed points, and (b) that the expansion is valid around the critical value of R, i.e. around R_0. The second assumption does not seem to be violated, at least not for the slightly sub/supercritical case, however, the first assumption is strongly violated by a solution which tends to infinity, starting at subcritical conditions when $\xi/r_0^2 < 1$. This condition implies $r_0^2 > \xi$, i.e. at a given subcritical value of R, as long as the initial conditions for r_0^2 are smaller than ξ ($r_0^2 < \xi$) the solution decays, spiralling towards the corresponding fixed point around which we applied the expansion. When the initial conditions satisfy $r_0^2 = \xi$ a solitary limit cycle solution around this fixed point exists (the terminology 'solitary limit cycle' is used to indicate that this limit cycle can be obtained only at $r_0^2 = \xi$). As the initial conditions move away from this fixed point and $r_0^2 > \xi$, the other fixed point may affect the solution as well, however, the asymptotic expansion used does not allow it, and it is because of this reason that the sol-

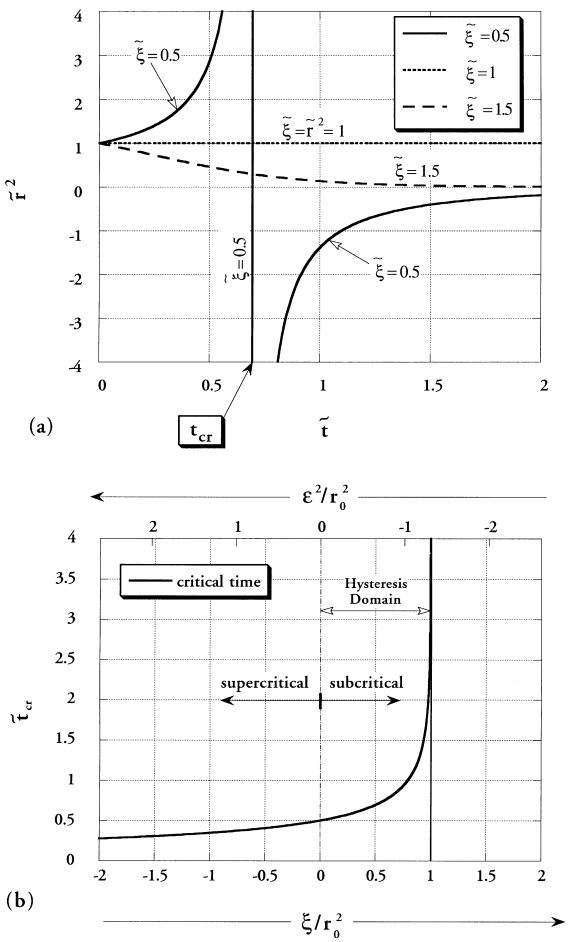

Fig. 2. (a) The amplitude solution for three values of $\tilde{\xi}$ corresponding to: (i) subtransitional conditions $\tilde{\xi}=1.5$; (ii) transitional conditions $\tilde{\xi}=\tilde{r}^2=1$; and (iii) supertransitional conditions $\tilde{\xi}=0.5$. (b) The variation of the critical time $\tilde{t}_{cr}$, when the amplitude solution diverges, as a function of $\tilde{\xi}$. Super/subcritical domains as well as the hysteresis domain are identified. The conversion of the independent variable for the top scale from $\tilde{\xi}$ to ε^2/r_0^2 corresponds to $Pr=10$, i.e. $\varphi=-1.30959$.

ution diverges, indicating the breakdown of the expansion used. While the divergence of the transient solution as $t\to t_{cr}$ (i.e. for $r_0^2>\xi$) indicates the breakdown of the assumed asymptotic expansion, it is sensible to suggest a physical interpretation of this result as the tendency of the solution to be repelled away from the neighbourhood of the present fixed point ($X_S=Y_S=Z_S=1$) towards the other fixed point ($X_S=Y_S=-1$; $Z_S=1$), or alternatively, its tendency to orbit around both fixed points, representing physically a homoclinic explosion.

We can imagine a process of gradually increasing the value of R towards R_0 (i.e. decreasing the value of ξ towards $\xi=0$). As we do so and we get closer to R_0 a wider range of initial conditions falls into the category which satisfies the solution's divergence condition. To the question of what solution would, therefore, exist when this condition is fulfilled one can anticipate (with hindsight of the computation results which are presented in the next section) that the solution may move towards the other fixed point, indicating a homoclinic explosion, or wander around both fixed points suggesting a chaotic solution. Transforming the condition for this transition to occur, from $r_0^2>\xi$, to the original physical parameters of the system by substituting the definitions of ξ and ε^2, one can observe that there is a value of $R\le R_0$, say R_t, beyond which the transition occurs, which can be expressed in the form

$$R_t = R_0(1-\mid\varphi\mid r_0^2) \tag{42}$$

where the minus sign and the absolute value of φ appear in order to show explicitly that $\varphi<0$ ($\varphi=-1.30959$ in the present case). If $R<R_t$ the solution decays, spiralling towards the corresponding fixed point, at $R=R_t$ we expect the solitary limit cycle solution, and beyond this transitional value of R, i.e. $R>R_t$, the solution moves away from this fixed point either (a) towards the other fixed point, or (b) wanders around both fixed points before it stabilises towards one of them, or (c) yields a chaotic behaviour by being attracted to the non-wandering set (Lorenz attractor). The present expansion cannot provide an answer to select between these three possibilities. However, it is important to stress that for any initial condition, $r_0^2\ll 1$, which we choose, we can find a value of $R\le R_0$ which satisfies eq. (42). At that value of R we expect to obtain a limit cycle solution and beyond it a possible chaotic solution.

To present the analytical solutions graphically the following rescaled variables relevant to Eqs. (37)–(41) are introduced: $\tilde{r}=r/r_0$, $\tilde{t}=r_0^2|\chi|t$ and $\tilde{\xi}=\xi/r_0^2$. Substituting these rescaled variables into Eqs. (37)–(41) transforms the solutions to the form in which they are plotted in Figs. 2(a) and (b). Fig. 2(a) shows an example of the amplitude solution [Eq. (37)] for three values of $\tilde{\xi}$, corresponding to subtransitional conditions (when $\tilde{\xi}>1$), transitional conditions (when $\tilde{\xi}=\tilde{r}^2=1$), and supertransitional conditions (when $\tilde{\xi}<1$ and the solution diverges at $\tilde{t}=\tilde{t}_{cr}$). The variation of the critical time $\tilde{t}_{cr}$ with $\tilde{\xi}$ is presented in Fig. 2(b) where one observes that the critical time tends to infinity as $\tilde{\xi}=(\xi/r_0^2)\to 1$. This fact suggests that it should not be difficult to recover numerically the solitary limit cycle solution around $\tilde{\xi}=(\xi/r_0^2)\approx 1$ as the time needed for this solution to be destabilised becomes very large in this neighbourhood (also see the Appendix), at least as long as the present analysis is valid, i.e. for values

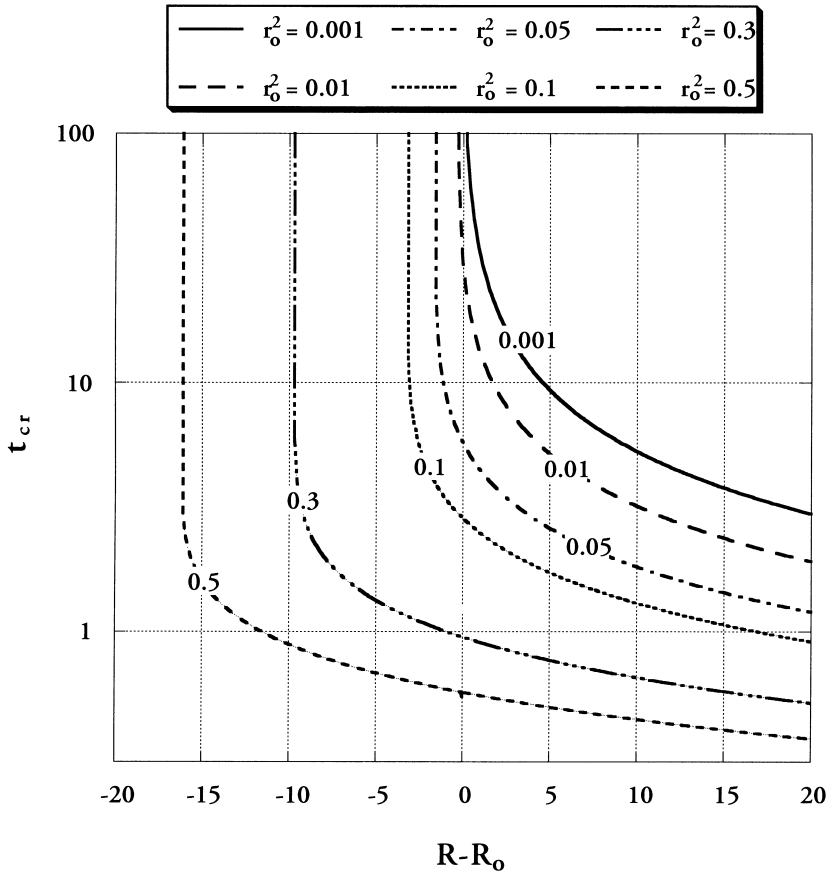

Fig. 3. The critical time as a function of $(R-R_0)$ for six values of initial conditions in terms of r_0^2. The transition from steady convection to chaos (or backwards) is linked to the existence (disappearance) of this critical time, explaining the mechanism for hysteresis.

of r_0^2 not too far away from one of the stationary points ($r_0^2 \ll 1$).

3.4. Hysteresis

Experimental and numerical results of transitions to chaos in the Lorenz system [9,10,2] suggest the existence of an hysteresis mechanism which is described as follows: when increasing the value of R gradually by approaching R_0 from below the transition to chaos occurs at $R = R_0$, while repeating the same procedure, but approaching R_0 from above, the transition from chaos to the stationary solution occurs at a value of $R < R_0$. We provide an explanation of the hysteresis phenomenon in connection with the transitional value of R which is presented in Eq. (42). Let us imagine a process of approaching R_0 from below, say $R < R_t$. This means that the initial conditions lead the solution to one of the convective fixed points, i.e. $r = 0$ (the fixed points represent the steady solutions of convective rolls moving clockwise or anticlockwise). As we gradually increase the value of R by starting the next experiment (or numerical procedure) with initial conditions taken from the post-transient previous solution obtained at the slightly lower value of R, the new initial conditions are very close to the fixed point, i.e. $r_0^2 \approx 0$ (they are not exactly at the fixed point because the post-transient values of the previous solution are reached asymptotically, and at any finite time there is a slight departure between the solution and the steady state), and according to Eq. (42) the corresponding transitional value R_t is very close to R_0. However, when one approaches R_0 from above, the initial conditions taken from the previous solution at a value of $R > R_0$ are quite large and far away from the fixed point (because they correspond to a chaotic solution obtained at a higher value of R), i.e. r_0^2 is far away from 0. Therefore, in such a case it is expected to obtain a chaotic solution for subcritical values of R until the value of R_t is reached from above, which this time it would be quite far away from R_0, according to Eq. (42). In graphical terms this process can be

observed in Fig. 2(b), where by moving towards R_0 from the left with not negligible initial conditions (r_0^2 is large) the transition is expected when the critical time disappears, i.e. at values of $R < R_0$, while by moving towards R_0 from the right and gradually decreasing the value of ξ with $r_0^2 \sim 0$, keeps the ratio ξ/r_0^2 greater than one, since when ξ approaches the origin, $\xi \to 0$ and $r_0^2 \to 0$ simultaneously. To make this explanation more transparent, the variation of the explicit critical time as a function of $(R-R_0)$, by using Eq. (39) and the definitions of ξ and ε^2, is presented in Fig. 3 for different values of r_0^2. The disappearance of the critical time at $R = R_t$ is an indication that the amplitude does not diverge, and therefore, a steady convective solution can be obtained. From the figure it is evident that for small values of r_0^2 (e.g. $r_0^2 = 0.001$), corresponding to the forward transition from steady convective to chaos, the asymptote of t_{cr} (i.e. the point when the critical time disappears) occurs very close to $R = R_0$, while for values of r_0^2 which are not so small, corresponding to the reverse transition from chaos to steady convection (e.g. $r_0^2 = 0.5$) the asymptote of t_{cr} occurs at values of $R < R_0$ which are quite far away from R_0. This explains the reason for observing hysteresis in the transition from steady convection to chaos and backwards, by using initial conditions corresponding to a previous solution at a slightly different values of R.

3.5. Breakdown of the asymptotic expansion

There are two possible ways for the breakdown of an assumed asymptotic expansion

1. First, it can breakdown in a smooth and gradual fashion, i.e. its solution becomes gradually less accurate quantitatively, and the shape of the orbit (e.g. for a Hopf bifurcation) departs gradually from the shape of the accurate solution. This route to the expansion breakdown, which still yields qualitatively valid results while quantitatively the error increases, applies when the underlying condition for the validity of the expansion, i.e. $\varepsilon \ll 1$, is gradually violated. Actually, the accurate form of this condition is $|\varepsilon^2|^{1/2} \ll 1$, in order to accommodate the subcritical domain for which $\varepsilon^2 < 0$. In the present case, the definition of ε as $\varepsilon^2 = (R-R_0)/R_0$ transforms this condition into $|R-R_0|^{1/2} \ll R_0^{1/2}$. For $R \cong R_t$ we can substitute Eq. (42) into the latter condition to yield $|r_0| \ll |\varphi|^{-1/2}$, and for $\varphi = -1.30959$, corresponding to the present case, it implies $|r_0| \ll 0.874$. This shows that the condition for the validity of the asymptotic expansion which originally constrained the values of R to be in the neighbourhood of R_0 is directly linked through the asymptotic solution to a consequent constraint on the initial conditions, r_0.
2. Second, a sharp breakdown of the asymptotic expansion which occurs as a singularity (or divergence) in the solution. In some cases this indicates a co-dimension-2 bifurcation. In the present case this occurs as $R \to R_t(r_0)$. When R moves slightly beyond R_t, i.e. $R > R_t$, the solution for r diverges via a singularity, representing the tendency of the solution to depart from the neighbourhood of the present fixed point towards the other convective fixed point, or to orbit around both, therefore, invalidating the asymptotic expansion used which, by using the complete solution of $X = 1 + \varepsilon r_1[\exp(i(\theta+\sigma_0)t) + \exp(-i(\theta+\sigma_0)t)] + O(\varepsilon^2)$, implies explicitly that $r = \varepsilon r_1$ is at a distance $O(\varepsilon)$ from the present fixed point ($X_S = Y_S = Z_S = 1$) but at a distance $O(1)$ from the other fixed point ($X_S = Y_S = -1$; $Z_S = 1$). In addition the non-linear interaction between the two solutions belonging to the two convective fixed points is prevented by the present expansion. However, as long as $R \leq R_t(r_0)$ the consistency of the expansion is not violated and the only way for the breakdown of the asymptotic expansion is smooth and gradual as formerly indicated in (1) above.

4. Adomian's decomposition method of solution

Adomian's decomposition method [5,6], is applied to solve the system of Eqs. (11)–(13). The method provides in principle an analytical solution in the form of an infinite power series for each dependent variable and its excellent accuracy in solving non-linear equations was demonstrated by Olek [12,13]. The solution follows Olek [13] and considers the following more general dynamical system of equations

$$\frac{dX_i}{dt} = \sum_{j=1}^{m} b_{ij} X_j + \sum_{l=1}^{m}\sum_{j=1}^{m} a_{ijl} X_j X_l, \qquad \forall i = 1, 2, \ldots, m \tag{43}$$

given the initial conditions $X_i(0)$, $i = 1, 2, \ldots, m$. It can be easily observed that the system of Eqs. (11)–(13) is just a particular case of Eq. (43). A detailed description of the method of solution is provided by Vadasz and Olek [7,8].

Olek [12,13] used the decomposition method to solve a variety of non-linear problems, some of which have closed form analytical solutions and a comparison was provided between the results obtained via the decomposition method and either exact analytical or numerical results. The conclusion from the comparison was that the decomposition method provided results which were accurate up to 14 significant digits. Even

when only three terms were kept in the decomposition series solution of the Lotka–Volterra equations the results agreed by at least five significant digits with a corresponding numerical solution. The problem can actually be solved to the desired accuracy by including more terms in the computation of the series.

For the system of Eqs. (43) the non-linear terms are of the rather simple X^2 form, so that very simple symmetry rules for the decomposition polynomials can be used. If we denote $\mathscr{L} \equiv \mathrm{d}/\mathrm{d}t$, the formal solution of (43) may be presented in the form

$$X_i(t) = X_i(0) + \mathscr{L}^{-1}\left[\sum_{j=1}^{m} b_{ij}X_j + \sum_{l=1}^{m}\sum_{j=1}^{m} a_{ijl}X_jX_l\right] \quad \forall i = 1, 2, \ldots, m \tag{44}$$

where $\mathscr{L}^{-1} \equiv \int_0^t [\,]\,\mathrm{d}t$. According to the decomposition method an expansion of the following form is assumed

$$X_i(t) = \sum_{n=0}^{\infty} \tilde{X}_{in} \quad \forall i = 1, 2, \ldots, m \tag{45}$$

Substituting (45) into (44) yields after rearranging the products

$$X_i(t) = X_i(0) + \mathscr{L}^{-1}\left[\sum_{j=1}^{m} b_{ij}\sum_{n=0}^{\infty}\tilde{X}_{jn} + \sum_{l=1}^{m}\sum_{j=1}^{m} a_{ijl}\sum_{n=0}^{\infty}\sum_{k=0}^{n}\tilde{X}_{jk}\tilde{X}_{l(n-k)}\right] \quad \forall i = 1, 2, \ldots, m \tag{46}$$

The solution is ensured by requiring

$$\tilde{X}_{i0} = X_i(0) \quad \forall i = 1, 2, \ldots, m \tag{47a}$$

$$\tilde{X}_{i1} = \mathscr{L}^{-1}\left[\sum_{j=1}^{m} b_{ij}\tilde{X}_{j0} + \sum_{l=1}^{m}\sum_{j=1}^{m} a_{ijl}\sum_{k=0}^{0}\tilde{X}_{jk}\tilde{X}_{l(0-k)}\right] \quad \forall i = 1, 2, \ldots, m \tag{47b}$$

$$\tilde{X}_{i2} = \mathscr{L}^{-1}\left[\sum_{j=1}^{m} b_{ij}\tilde{X}_{j1} + \sum_{l=1}^{m}\sum_{j=1}^{m} a_{ijl}\sum_{k=0}^{1}\tilde{X}_{jk}\tilde{X}_{l(1-k)}\right] \quad \forall i = 1, 2, \ldots, m \tag{47c}$$

$$\vdots$$

$$\tilde{X}_{in} = \mathscr{L}^{-1}\left[\sum_{j=1}^{m} b_{ij}\tilde{X}_{j(n-1)} + \sum_{l=1}^{m}\sum_{j=1}^{m} a_{ijl}\sum_{k=0}^{n-1}\tilde{X}_{jk}\tilde{X}_{l(n-k-1)}\right] \quad \forall i = 1, 2, \ldots, m \tag{47d}$$

After carrying out the integrations, the following solution is obtained

$$X_i(t) = \sum_{n=0}^{\infty} c_{i,n}\frac{t^n}{n!} \quad \forall i = 1, 2, \ldots, m \tag{48}$$

where

$$c_{i,0} = X_i(0) \quad \forall i = 1, 2, \ldots, m \tag{49}$$

and the general term for $n \geq 1$ is defined through the following recurrence relationship

$$c_{i,n} = \sum_{j=1}^{m} b_{ij}c_{j,(n-1)} + (n-1)!\sum_{l=1}^{m}\sum_{j=1}^{m}\sum_{k=0}^{n-1} a_{ijl}\frac{c_{j,k}}{k!}\frac{c_{l,(n-k-1)}}{(n-k-1)!} \quad \forall i = 1, 2, \ldots, m \tag{50}$$

The decomposition method does not assure, on its own, existence and uniqueness of the solution. Furthermore, the convergence of the series (48) is also difficult to assess a priori. In any case the practical need to compute numerical values for the solution at different values of t requires the truncation of the series and, therefore, its convergence needs to be established in each particular case. To achieve this goal, the decomposition method can be used as an algorithm for the approximation of the dynamical response in a sequence of time intervals $[0, t_1)$, $[t_1, t_2)$, $\ldots$, $[t_{n-1}, t_n)$ such that the solution at t_p is taken as initial condition in the interval $[t_p, t_{p+1})$ which follows. This approach has the following advantages: (i) in each time-interval one can apply a theorem proved by Répaci [14], which states that the solution obtained by the decomposition method converges to a unique solution as the number of terms in the series becomes infinite; and (ii) the approximation in each interval is continuous in time and can be obtained with the desired accuracy corresponding to the desired number of terms. The latter procedure is adopted in the computation of the solution to Eqs. (11)–(13). Therefore, although the Adomian's decomposition method provides an analytical form for the solution, the practical need to obtain numerical values from the infinite power series, and consequently the series truncation, and the practical procedure to accomplish this task, transform the otherwise analytical results into a computational solution achieved up to a finite accuracy. We will refer to the results belonging to this solution's results as 'computational results' (as distinct from 'numerical') to stress the fact that they are obtained from an analytical solution which needed to be computed up to a finite accuracy.

One can easily observe that Eqs. (11)–(13) are just a particular case of Eqs. (43) with $m = 3$. This set of equations provides the following non-zero coefficients for substitution in Eq. (43): $b_{11} = -Pr$; $b_{12} = Pr$; $b_{21} = R$; $b_{22} = -1$; $b_{33} = -\lambda$; $a_{213} = -(R-1)$; $a_{312} = \lambda$. Except for these coefficients all others are identically zero. Therefore, the coefficients $c_{i,n}$, in Eq. (50) take

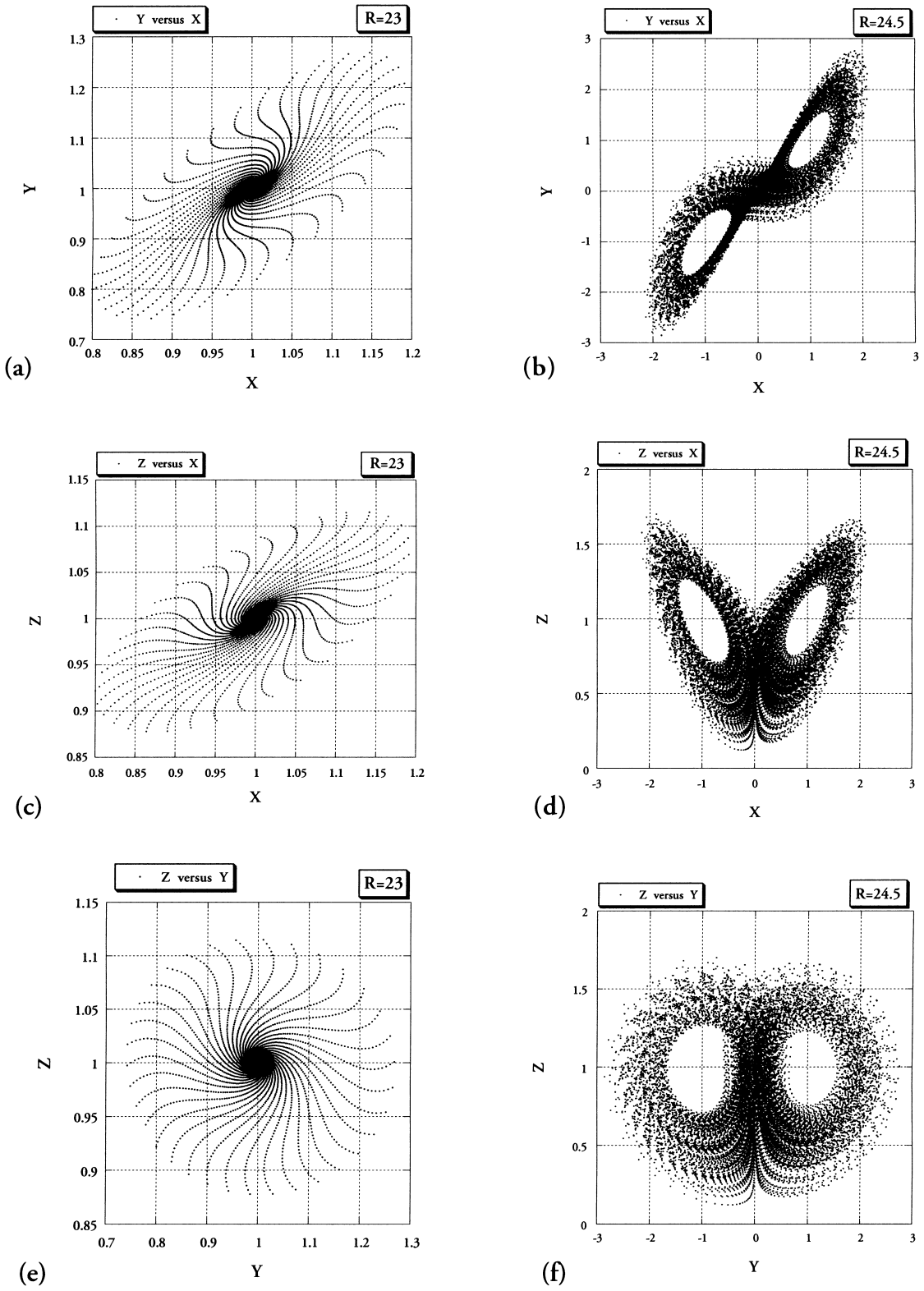

Fig. 4. The computational results for the evolution of trajectories over time in the state space for two values of Rayleigh number (in terms of R). Initial conditions: $X^{(0)} = Y^{(0)} = 0.8$ and $Z^{(0)} = 0.92195$ (solution data points not connected). (a) Projection of trajectories onto the Y–X plane for $R = 23$. (b) Projection of post-transient trajectories onto the Y–X plane for $R = 24.5$. (c) Projection of trajectories onto the Z–X plane for $R = 23$. (d) Projection of post-transient trajectories onto the Z–X plane for $R = 24.5$. (e) Projection of trajectories onto the Z–Y plane for $R = 23$. (f) Projection of post-transient trajectories onto the Z–Y plane for $R = 24.5$

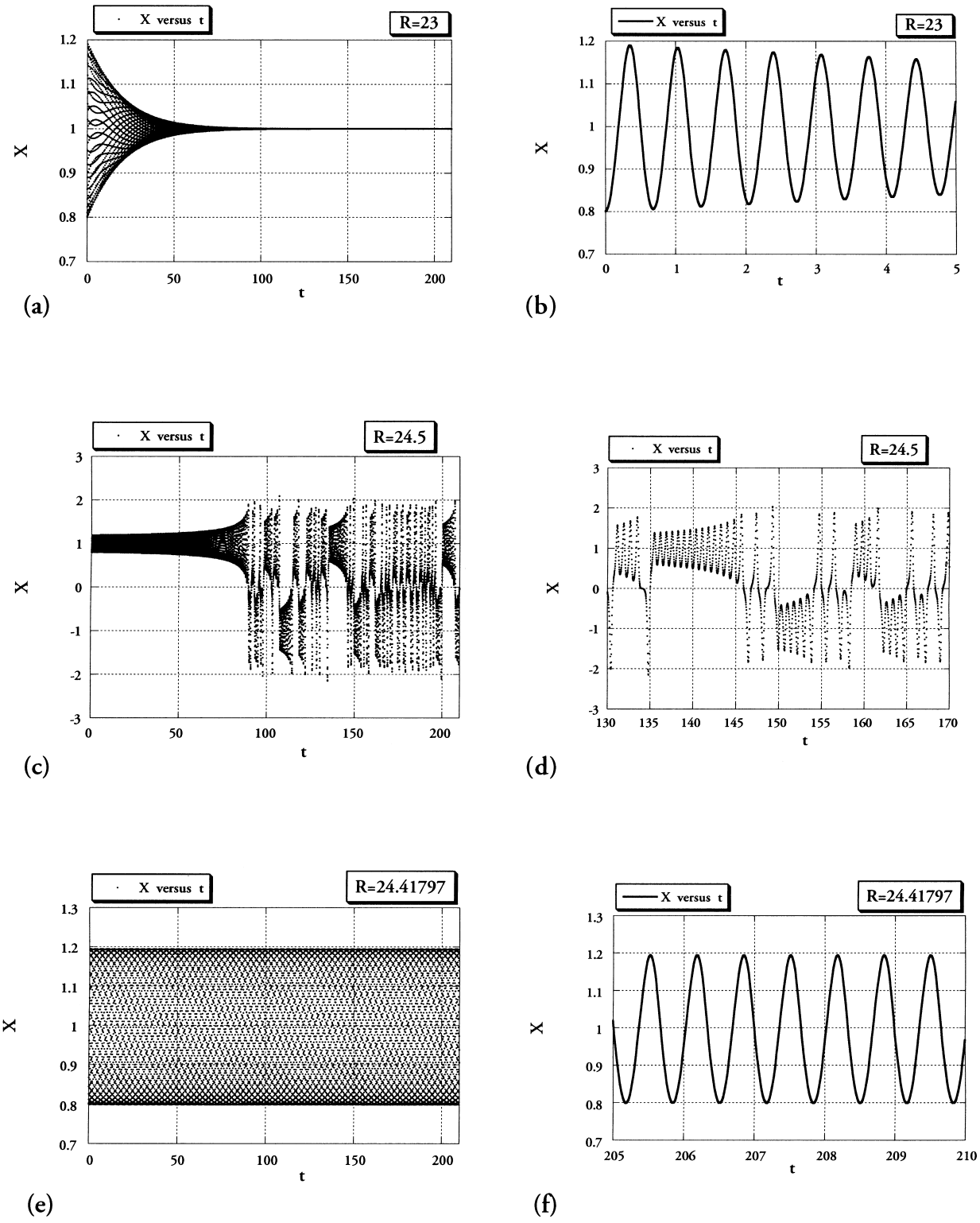

Fig. 5. The computational results for the evolution of $X(t)$ in the time domain for three values of the Rayleigh number (in terms of R). (a) X as a function of time for $R = 23$; the solution stabilises to the fixed point. (b) The inset of Fig. 7(a) detailing the oscillatory decay of the solution (data points are connected). (c) X as a function of time for $R = 24.5$; the solution exhibits chaotic behaviour. (d) The inset of Fig. 7(c) detailing the chaotic solution. (e) X as a function of time for $R = 24.41797$; the solution is periodic. (f) The inset of Fig. 7(e) detailing the periodic solution (data points are connected).

the particular form

$$c_{1,\,n} = -Pr(c_{1,\,(n-1)} - c_{2,\,(n-1)}) \tag{51a}$$

$$c_{2,\,n} = Rc_{1,\,(n-1)} - c_{2,\,(n-1)} - (R-1)\sum_{k=0}^{n-1}\frac{(n-1)!c_{1,\,k}c_{3,\,(n-k-1)}}{k!(n-k-1)!} \tag{51b}$$

$$c_{3,\,n} = -\lambda c_{3,\,(n-1)} + \lambda\sum_{k=0}^{n-1}\frac{(n-1)!c_{1,\,k}c_{2,\,(n-k-1)}}{k!(n-k-1)!} \tag{51c}$$

In all computations 15 terms in the series and a time interval of $\Delta t = 10^{-3}$ were used, and all computations were performed up to a post-transient value of $t = t_{\max} = 210$. All computations were carried out to double-precision on an Apple Power Macintosh computer (G3 upgrade) and the elapsed time for each computation corresponding to a particular value of R and a particular set of initial conditions was ~12 s. While the value of R as well as the initial conditions vary from one computation to another, the value of Pr is kept constant at $Pr = 10$. This value of $Pr = 10$ yields the critical values: $R_0 = 470/19 \cong 24.737$, $\sigma_0^2 = 1760/19 \cong 92.63$ and the following values for the amplitude equation coefficients [in Eq. (34)] $\varphi = -1.30959$ and $\beta = 0.747609$.

In order to compare the computational results to the analytical ones obtained in Section 3 via the weak non-linear theory we have to make sure that the initial conditions for the computations are consistent with the initial conditions corresponding to the weak non-linear solution. It should be pointed out that the set of possible initial conditions in the weak non-linear solution (37) and (38) is constrained because we did not include the decaying solutions of the form $a_{12}(\tau)\exp(\sigma_3 t)$ (with $\sigma_3 < 0$ and real) in Eq. (20). Therefore, this constraint, which is equivalent to setting $(a_{12})_{\tau=0} = 0$ and $(\theta)_{\tau=0} = 0$, is kept valid for all computational results as well. The present weak non-linear solution provides the following conditions which are necessary and sufficient to ensure the consistency of the initial conditions between the weak non-linear and computational solutions

$$\begin{aligned} X^{(0)} &= Y^{(0)} = 1 + 2r_0; \\ Z^{(0)} &= 1 + \frac{\sigma_0^2}{Pr(R_0-1)}[X^{(0)} - 1] \\ &= 1 + \frac{2\sigma_0^2}{Pr(R_0-1)}r_0 \end{aligned} \tag{52}$$

where $X^{(0)}$, $Y^{(0)}$ and $Z^{(0)}$ are the initial conditions for X, Y and Z, respectively, and r_0 is the initial condition for r, as used in the weak non-linear solution in Section 3. Furthermore, using Eq. (52) it is noted that $r_0 = (X^{(0)} - 1)/2 = (Y^{(0)} - 1)/2$. Clearly this yields negative values of r_0 if $X^{(0)} < 1$ or $Y^{(0)} < 1$. We, therefore, extend the definition of r and allow it to take negative values. This is equivalent to a phase shift in the limit cycle solution of the form $\tilde{\theta} = \theta + \pi$ and can be rigorously justified. For r_0 this corresponds to a phase shift $\tilde{\theta}_0 = \theta_0 + \pi = \pi$, because $\theta_0 = (\theta)_{\tau=0} = 0$, implicitly in the present case.

5. Results and discussion

Before presenting the comparison between the computational and weak non-linear analytical results a brief sequence of computational results are presented in Figs. 4 and 5 to demonstrate the transition from a steady convection to chaos. These results correspond to initial conditions consistent with $r_0 = -0.1$ ($X^{(0)} = Y^{(0)} = 0.8$ and $Z^{(0)} = 0.92195$) and are presented at two values of R, the first at $R = 23$ just before the transition to chaos occurs, and the second just after the transition, at $R = 24.5 < R_0$ (note that $R_0 \cong 24.74$). The results in terms of projections of trajectories data points on the Y–X, Z–X and Z–Y planes are presented in Fig. 4, where the trajectories data points were not connected. It can be observed from Fig. 4(a), (c) and (e) that for $R = 23$, the solution's trajectories spiral towards the fixed point resulting in a steady convection. However, the post-transient solution's trajectories at $R = 24.5$ presented in Fig. 4(b), (d) and (f) exhibit a typical chaotic behaviour. The results for the same two values of R in the time domain are presented in Fig. 5 for X as a function of t. The decay of the solution corresponding to $R = 23$ towards the steady state value of $X = 1$ is clearly identified in Fig. 5(a) and the inset (where the data points are connected) presented in Fig. 5(b) highlights its oscillatory behaviour. On the other hand, for $R = 24.5$, Fig. 5(c) shows a typical chaotic result and the inset presented in Fig. 5(d) focuses on the post-transient time domain $130 < t < 170$. It is worth emphasising the fact that the computational results show a transition to chaos at a subcritical value of R (the critical value of $R_0 \cong 24.74$). A comparison between Figs. 5(a) and (c) at a common transient time domain $0 < t < 50$ shows that the envelope of the function $X(t)$ converges for $R = 23$ (Fig. 5(a)) and diverges for $R = 24.5$ (Fig. 5(c)). This suggests that somewhere in-between $R = 23$ and $R = 24.5$ the envelope of the function $X(t)$ will neither converge nor diverge, producing a typical limit cycle. Looking for this limit cycle provides the result presented in Fig. 5(e), where it is evident that the envelope of the function $X(t)$ does not converge nor diverge, and the inset presented in Fig. 5(f) (where the data points are con-

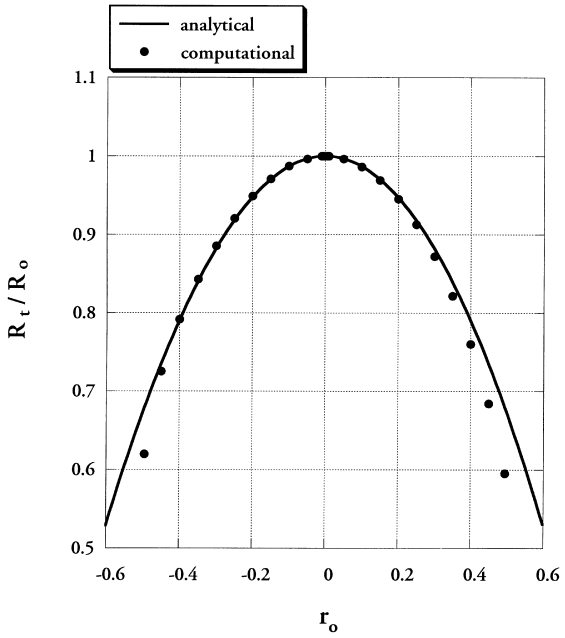

Fig. 6. Transitional subcritical values of Rayleigh number in terms of R_t/R_0 as a function of the initial conditions r_0. A comparison between the weak non-linear solution (— analytical) and the computational results (● computational).

nected) demonstrates the periodic behaviour of the solution.

The objective in the presentation of the following results is to demonstrate the appearance of this solitary limit cycle at particular values of R prior to the transition to chaos (here a 'solitary limit cycle' is used in connection to the fact that it appears at a particular value of $R=R_t$ and only at this particular value of R; no relationship to solitons is suggested) and to present the computational values of $R=R_t$ where this transition occurs [the analytical values of R_t were presented in Section 3, see Eq. (42)] for different initial conditions (consistent with the weak non-linear solution). It should be stressed that this limit cycle was obtained computationally irrespective of whether the initial conditions were consistent with the weak non-linear solution or not; the consistency is imposed only for quantitative comparison purposes. A sequence of numerous computations were performed in order to evaluate these transitional R values.

The results are presented in Fig. 6 where the continuous curve represents the analytical solution expressed by Eq. (42) while the dots represent the computational results. The very good agreement between the analytical and computational solutions in the neighbourhood of the convective fixed point (i.e. $|r_0|\ll 1$) is evident from Fig. 6.

As the initial conditions move away from the convective fixed point and the value of $|r_0|$ increases the analytical solution departs from the computational results, which reconfirms the validity of the weak non-linear solution in the neighbourhood of a convective fixed point and its breakdown far away from this point. The relative difference between the two solutions, i.e. the value of $|(R_t/R_0)_{analyt.}-(R_t/R_0)_{comp.}|/(R_t/R_0)_{comp.}$, is insignificantly small (less than 1%) for $|r_0|<0.3$, and equals 1.16% at $r_0=0.3$, 2.2% at $r_0=0.35$, 3.97% at $r_0=0.4$, 7.38% at $r_0=0.45$, 9.6% at $r_0=-0.495$, and 14.1% at $r_0=0.495$. The departure between the computational results and the analytical ones is clearly not symmetrical with respect to $r_0=0$. While the weak non-linear solution is symmetrical with respect to $r_0=0$, due to its elliptical shape, there is no reason to expect this symmetry from a computational solution as one moves away from the fixed point (the symmetry is kept for $|r_0|\ll 1$). The maximum value of $|r_0|$ for which we could obtained results and still be consistent with the weak non-linear solution (around one of the fixed points) was $r_0=\pm 0.5$. Actually at $r_0=-0.5$ the corresponding initial conditions are $X^{(0)}=Y^{(0)}=0$ and $Z^{(0)}=0.609756$ which lie on the Z-axis that is included on the stable manifold of the origin. Therefore, the computational results obtained for this set of initial conditions lead naturally to the origin producing the motionless solution. Furthermore, in the neighbourhood of $r_0=\pm 0.5$ one expects to find the homoclinic orbit. In order to evaluate the solitary limit cycle as we approach $r_0=-0.5$ we evaluated the computational solution at $r_0=-0.495$. Another interesting result from the computations is the fact that it was relatively very easy to detect the solitary limit cycle when the initial conditions were close to the convective fixed point, i.e. around $r_0=0$. There, the critical time is very large, as established via the weak non-linear analysis, and if the value of R is sufficiently close to R_t the limit cycle appears and persists. The relatively easy computational recovery of the solitary limit cycle does not imply that this limit cycle is stable. On the contrary, a slight variation of the initial conditions causes a change in the value of R_t and consequently the limit cycle disappears. It can be recovered again by a further adjustment of the value of R [see Eq. (42)]. Naturally, in this neighbourhood the accuracy in estimating the value of R_t is somewhat compromised because of the same reason. Nevertheless, if the maximum time for presenting the solution (i.e. t_{max}) is sufficiently large this accuracy problem around $r_0=0$ can be resolved. In our case, with $t_{max}=210$, the results provided accurate values of R_t. However, as we move away from the neighbourhood of $r_0=0$ by using initial conditions further away from the convective fixed point, it becomes more and more difficult to detect the solitary limit cycle, and more computations are needed by modifying the value of R closer and closer to R_t.

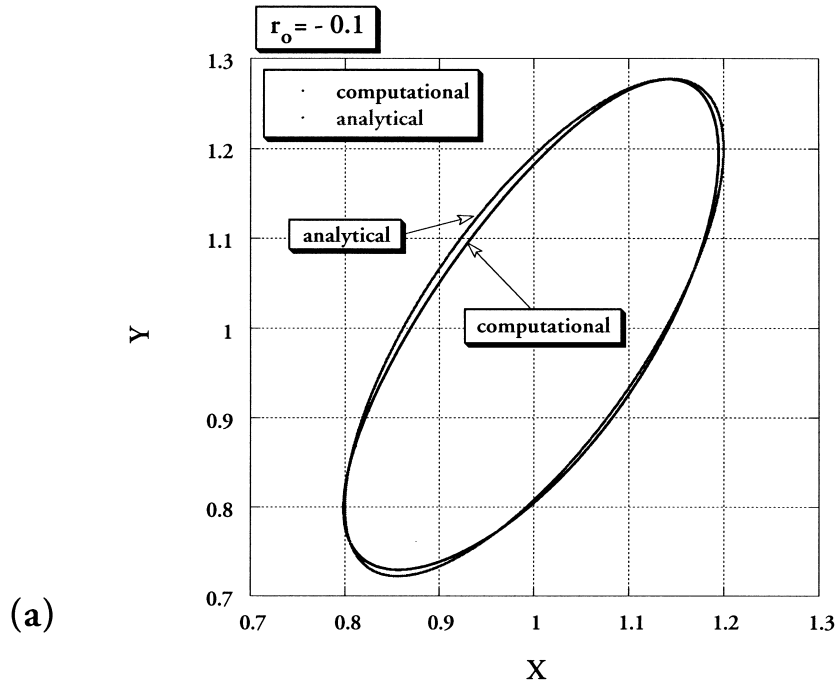

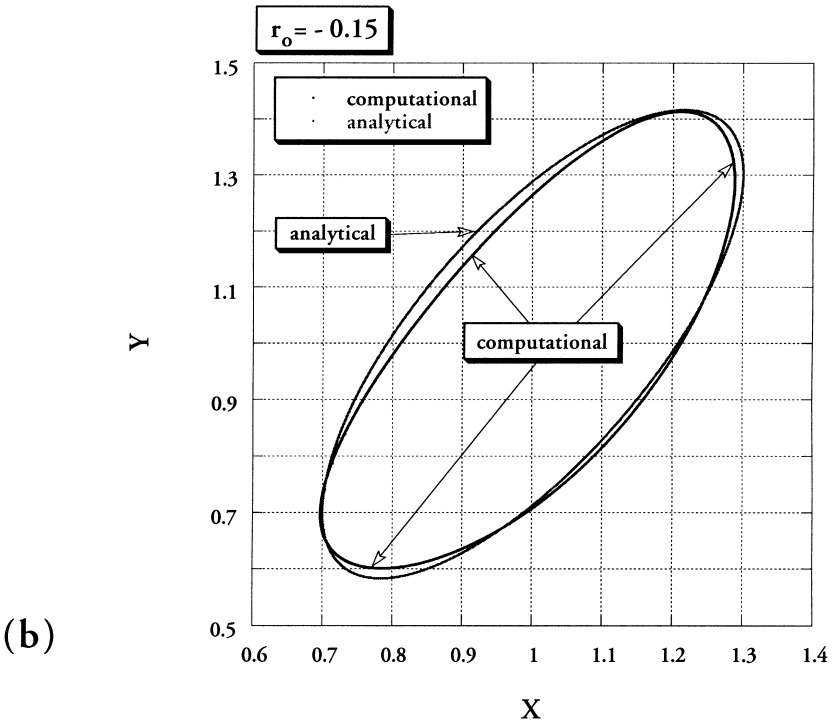

Fig. 7. Comparison between the computational and analytical results for the solitary limit cycle in terms of post-transient trajectories data points projected onto the Y–X plane, for different values of r_0. (a) Initial conditions: $r_0 = -0.1$. (b) Initial conditions: $r_0 = -0.15$.

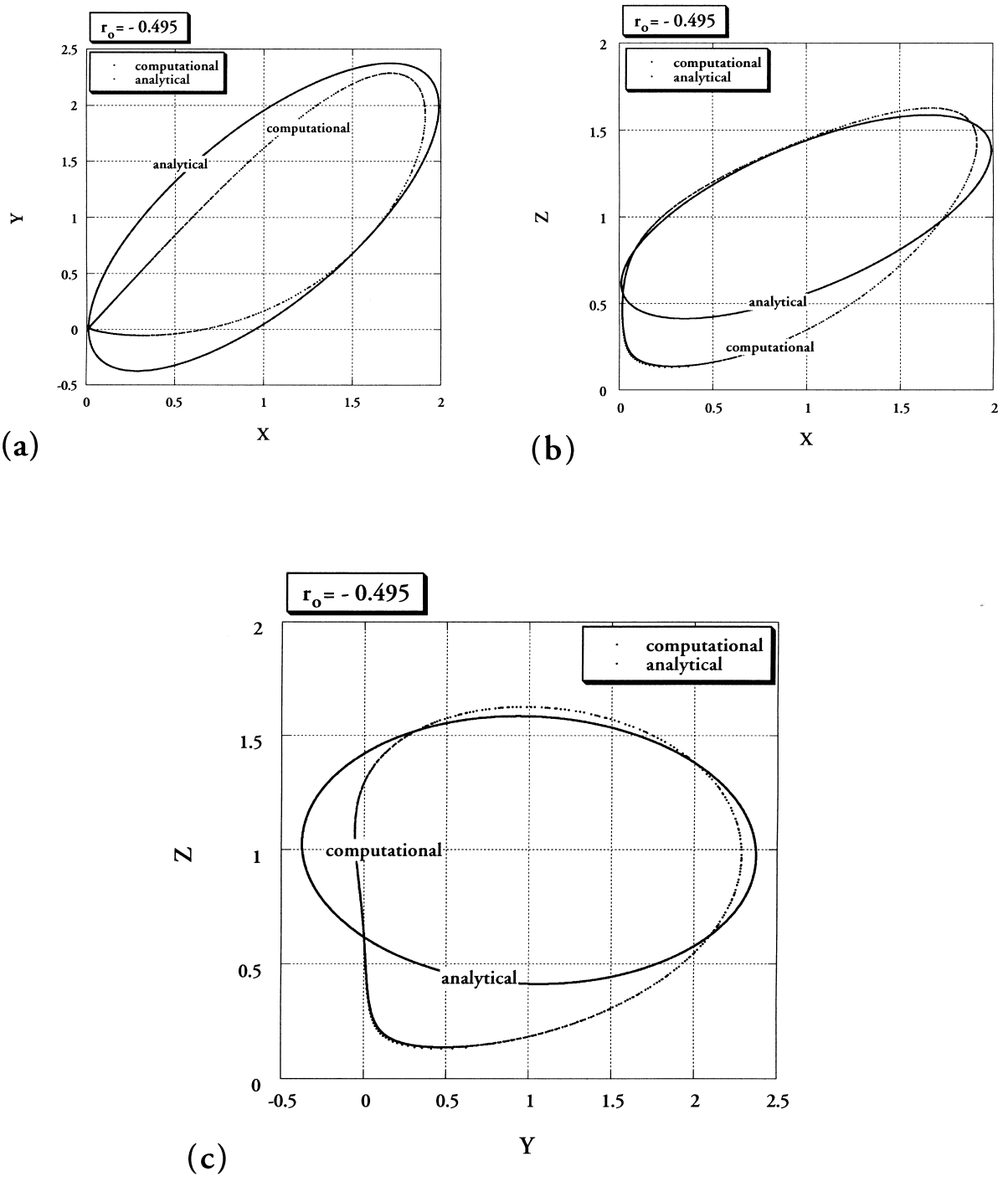

Fig. 8. Comparison between the computational and analytical results of the solitary limit cycle for initial conditions far away from the convective fixed point and corresponding to $r_0 = -0.495$. (a) Trajectories data points projected onto the Y–X plane. (b) Trajectories data points projected onto the Z–X plane. (c) Trajectories data points projected onto the Z–Y plane.

While detecting the solitary limit cycle becomes more difficult as the initial conditions move away from the convective fixed point, the accuracy of the value of R_t once the limit cycle was detected becomes extremely high. For example, at $r_0 = -0.2$ the limit cycle appeared at $R = R_t = 23.474475752$. The need to use 11 significant digits in order to obtain the limit cycle solution over the whole time domain just emphasises the difficulty of detecting the limit cycle as one moves away from the convective fixed point and the associated accuracy in evaluating R_t. This is also an indication that this limit cycle becomes less and less stable as one departs from the neighbourhood of the convective fixed point. As one moves even further away, more significant digits are required in order to establish the value of R_t and detect the limit cycle over the whole time domain, and when this process reaches the limit of over 14 digits, which corresponds to the double-precision computation, the limit cycle cannot be detected for the whole time domain selected.

All computational orbits evaluated yielded post-transient solutions which persisted for a very long time (attempting to increase the value of t_{max} beyond $t_{max} = 210$ significantly, did not change the periodic result), except for the orbits corresponding to $r_0 = -0.3$ and $r_0 = -0.495$ where the solutions stabilised to the convective fixed point $X = Y = Z = 1$ (or experienced a homoclinic explosion if the value of R was slightly increased) after a relatively long period of time during which the periodic orbit persisted.

A further comparison between the computational and analytical results is presented in Figs. 7 and 8. The solitary limit cycle corresponding to the complete weak non-linear solution is presented in Fig. 7 together with the corresponding computational solution in terms of trajectories data points projected on the Y–X plane. The trajectories data points were not connected. Fig. 7(a) corresponds to initial conditions of $r_0 = -0.1$ while Fig. 7(b) corresponds to $r_0 = -0.15$. In both cases it can be observed that the analytical and computational limit cycles are quite close. The corresponding projections on the Z–X and Z–Y planes (not presented here) show that the analytical and computational solutions almost overlap. Similarly, the limit cycle solutions corresponding to values of $|r_0|$ smaller than 0.1 show that the analytical and computational results overlap and are, therefore, not presented graphically here. On the other hand, the solitary limit cycle solutions corresponding to $r_0 = -0.495$, i.e. quite far away from the convective fixed point, are presented in Fig. 8 in terms of trajectories data points projected on the Y–Z, Z–X and Z–Y planes. The comparison between the analytical and computational limit cycle results presented in Fig. 8 show a marked departure between the two solutions, not only in the quantitative sense as presented by the deviation of the computational value of R_t from its predicted analytical value (see Fig. 6), but also qualitatively their shapes are substantially different. While the analytical periodic orbit maintains its elliptical shape similar regardless of r_0, the computational results show that as the solitary limit cycle approaches conditions consistent with the homoclinic orbit its shape is altered considerably (the shape of the homoclinic orbit is by far different than that of an ellipse, see Vadasz [15]).

6. Conclusions

The investigation of the route to chaos in a fluid layer heated from below was presented by using the weak non-linear theory and Adomian's decomposition method to provide solutions to a truncated Galerkin representation of the governing equations, which is identical to Lorenz equations. Both the analytical and computational results confirmed the transition from steady convection to chaos via a solitary limit cycle at a subcritical value of the Rayleigh number. The subcritical transition was explained by investigating the transient amplitude solution results obtained via the weak non-linear theory. This investigation sheds some light in explaining the experimentally well-known phenomenon of hysteresis. Comparison between the computational and analytical results shows very good quantitative as well as qualitative agreement in the neighbourhood of any one (but only one) of the convective steady solutions. The weak non-linear solution diverges as the initial conditions move away from the neighbourhood of the convective fixed point. Under these conditions the asymptotic expansion used breaks down as it cannot accommodate a solution which is affected by both convective fixed points because these points are far apart in terms of the expansion used. It is suggested that another expansion be used which brings both fixed points closer to each other. Then the possibility of a co-dimension-2 bifurcation where the limit cycle corresponding to each one of the convective fixed points resonate each other should be investigated.

Acknowledgements

The author wishes to thank the Foundation for Research Development (South Africa) for partially supporting this study through the Competitive Industry Research Grant (CIPM-GUN2034039).

Appendix A. Linear stability analysis of the amplitude solution

A linear stability analysis of the amplitude solution

is presented in this Appendix in order to clarify the reason for the relatively easy computational recovery of the 'solitary limit cycle' around $R \approx R_t$, when $r_0^2 \ll 1$. The post-transient solution of the amplitude Eq. (36), $r_b = \pm \xi^{1/2}$, is taken as the basic solution of which stability is investigated. Introducing small perturbations around this basic solution in the form: $r = r_b + \delta r^{(1)}$, where $\delta \ll 1$, and substituting this form of perturbed solution in to Eq. (36) yields an equation for the perturbation in the form

$$\frac{dr^{(1)}}{dt} = -2\chi r_b^2 r^{(1)} \tag{A1}$$

Introducing in (A1) the basic solution $r_b^2 = \xi$ and the absolute value of χ to indicate explicitly the already established fact that $\chi < 0$ yields

$$\frac{dr^{(1)}}{dt} = 2 \mid \chi \mid \xi r^{(1)} \tag{A2}$$

The solution to Eq. (A2) has the form

$$r^{(1)} = A \ \exp[2 \mid \chi \mid \xi t] \tag{A3}$$

indicating that for $R < R_0$ (i.e. $\xi > 0$) the basic solution r_b is unstable. However, at $R = R_t < R_0$, where the limit cycle is detected $\xi = r_0^2$ [see complete discussion following Eq. (41) and Fig. 2(a)]. Replacing the latter relationship into Eq. (A3) yields

$$r^{(1)} = A \ \exp[2 \mid \chi \mid r_0^2 t] \tag{A4}$$

From Eq. (A4) it is evident that for $r_0^2 \ll 1$ (with $|\chi| = 1.7517$) the relative growth rate of a perturbation around the basic solution in the neighbourhood of R_t is very small, i.e. $(2|\chi| r_0^2) \ll 1$, and the time needed for the limit cycle to be destabilised becomes very long, thus allowing its computational recovery.

References

[1] E.N. Lorenz, Deterministic non-periodic flows, J. Atmos. Sci. 20 (1963) 130–141.

[2] C. Sparrow, The Lorenz Equations: Bifurcations, Chaos, and Strange Attractors, Springer-Verlag, New York, 1982.

[3] A.J. Lichtenberg, M.A. Liberman, Regular and Chaotic Dynamics, 2nd ed., Springer-Verlag, New York, 1992.

[4] W.V.R. Malkus, Non-periodic convection at high and low Prandtl number, Mem. Soc. R. Sci. Liege IV (6) (1972) 125–128.

[5] G. Adomian, A review of the decomposition method in applied mathematics, J. Math. Anal. Appl. 135 (1988) 501–544.

[6] G. Adomian, Solving Frontier Problems in Physics: The Decomposition Method, Kluwer, Dordrecht, 1994.

[7] P. Vadasz, S. Olek, Weak turbulence and chaos for low Prandtl number gravity driven convection in porous media, Transport in Porous Media 37(1) 1999 69–91.

[8] P. Vadasz, S. Olek, Transitions and chaos for free convection in a rotating porous layer, Int. J. Heat Mass Transfer 14 (11) (1998) 1417–1435.

[9] Y. Wang, J. Singer, H.H. Bau, Controlling chaos in a thermal convection loop, J. Fluid Mechanics 237 (1992) 479–498.

[10] P. Yuen, H.H. Bau, Rendering a subcritical Hopf bifurcation supercritical, J. Fluid Mechanics 317 (1996) 91–109.

[11] P. Vadasz, Local and global transitions to chaos and hysteresis in a porous layer heated from below, Transport in Porous Media 1999 (in press).

[12] S. Olek, An accurate solution to the multispecies Lotka–Volterra equations, SIAM Review 36 (1994) 480–488.

[13] S. Olek, Solution to a class of nonlinear evolution equations by Adomian's decomposition method. Manuscript in preparation, 1997.

[14] A. Répaci, Non-linear dynamical systems: on the accuracy of Adomian's decomposition method, Appl. Math. Lett. 3 (1990) 35–39.

[15] P. Vadasz, On the homoclinic orbit for convection in a fluid layer heated from below, Int. J. Heat and Mass Transfer 42 (1999) 3557–3561.